Effect of rod-to-grain angle on capacity and stiffness of axially and laterally loaded long threaded rods in timber joints

Martin Cepelka[1*], Kjell Arne Malo[1**], Haris Stamatopoulos [1***]

[1] Department of Structural Engineering, Norwegian University of Science and Technology (NTNU), Rich. Birkelandsvei 1A, 7491, Trondheim, Norway

[*] corresponding author, martin.cepelka@ntnu.no , +4795409031

[**] kjell.malo@ntnu.no

[***] haris.stamatopoulos@ntnu.no

Abstract

Long threaded rods have recently been widely used as a reinforcement of glued laminated timber in perpendicular to the grain direction. The recent research has thus focused mainly on the withdrawal properties of the threaded rods in the axial direction. Utilizing their large withdrawal stiffness and strength, the threaded rods can also effectively be used as connectors in moment resisting timber joints. Yet, in joints, the threaded rods are often imposed to a non-axial loading, due to inclination of the rod axis to the grain as well as loading direction different from the rod axis. No design models are currently available for the combined axial and lateral loading of the threaded rods. In the present work, the effects of the rod-to-grain and load-to-rod angles on capacity and stiffness of the threaded rods are investigated by use of experiments and finite element models. Based on those, analytical expressions for determining stiffness and capacity of axially and laterally loaded threaded rods are proposed, intended as a basis for practical joint design. Furthermore, effect of various boundary conditions applied at the rod-ends is studied.

Keywords: long threaded rod, timber joint, combined axial and lateral loading, glulam, 3D finite element model, capacity, stiffness

1. Introduction

The recently erected 14-storey timber building in Bergen in Norway – Treet, demonstrates new possibilities in the modern timber engineering design (Malo et al. 2016). The load-bearing structure consists of glulam column-beam trusses with slotted-in steel plates and dowels used in joints. The stability of the structure is ensured by diagonal components in the trusses. Alternatively, the horizontal stiffness of buildings can be enhanced by increased rotational stiffness in joints that also enables larger spans between columns. Compared to buildings made of massive cross-laminated panels (CLT), the glulam frames provide an open interior and thus more flexibility for architects and building owners.

Joints with large rotational stiffness can be obtained by use of long threaded rods (Malo and Stamatopoulos 2016). The rods are often inclined with respect to grains, as illustrated in Fig. 1. This allows accommodating longer rods in columns, and decreases risk for loss of capacity in beams, due to longitudinal shrinkage cracks in close proximity to the rods. The

long threaded rods feature high withdrawal stiffness and capacity in the axial direction. However, the inclination of the rods, as well as simultaneous bending and shear actions in the joints, results in combined axial and lateral loading of the rods, which decreases their capacity and stiffness. Therefore, the designer must choose an optimal inclination of the rods. Currently, there are no available models for long threaded rods accounting for combined axial and lateral loading. The withdrawal properties of long threaded rods for pure axial load were studied by Blaß and Krüger (2010) and Stamatopoulos and Malo (2015); (2016). Several studies were conducted for timber-to-timber joints with inclined self-tapping screws, see e.g. (Bejtka and Blaß 2002; Tomasi et al. 2010; Jockwer et al. 2014). In addition, few design guidelines generally valid for screws are given by Eurocode 5 (CEN 2004).

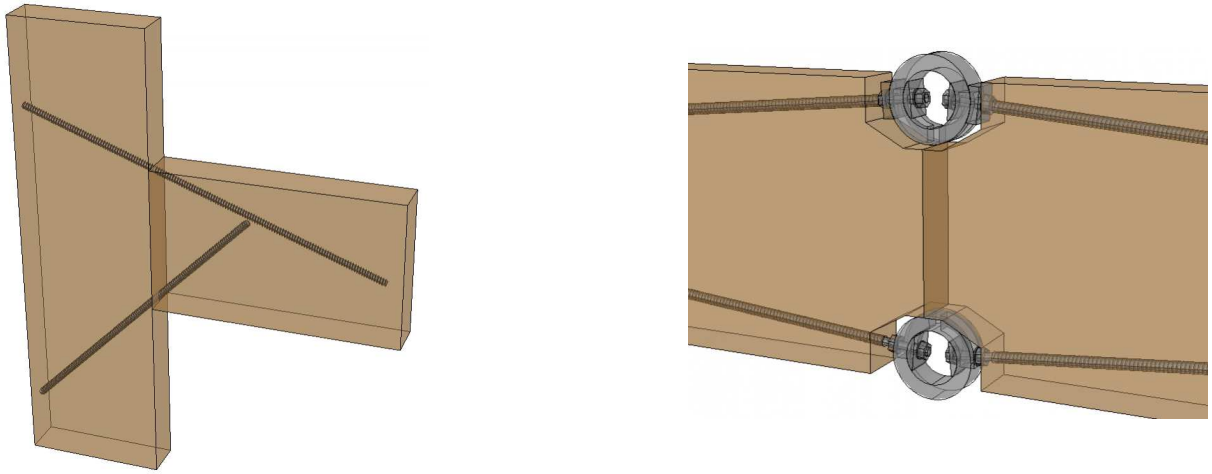

Fig. 1 Prototype timber joints by use of long threaded rods

Long threaded rods are similar to self-tapping screws in terms of material properties and geometry. The threaded part is produced by rolling or forging the wire rod, which results in steel hardening and thus increased strength. Self-tapping screws feature diameters up to 12-14 mm, and they are usually driven to timber without pre-drilling. The threaded rods feature diameters larger than 15 mm (usually 16-20 mm) and they are driven into pre-drilled holes of a diameter corresponding to the core diameter of the rods. Due to the similarities between self-tapping screws and threaded rods, some models developed for screws may potentially be applied for long threaded rods. However, most of the current models proposed for screws are based on a curve fitting to experimental results and it is generally not possible to apply them outside their validity range. In addition, in contrast to self-tapping screws, long threaded rods feature different detailing at the rod-ends when used in timber joints (see examples in Fig. 1), which should be respected in the analytical model. Therefore, in the present work, the effects of rod-to-grain and load-to-rod angles on capacity and stiffness of long threaded rods are investigated by use of experiments and numerical models. An assessment of the applicability of the capacity prediction by Eurocode 5 (CEN 2004), and by the model proposed by Jockwer et al. (2014) for self-tapping screws, is carried out on basis of the experimental results. An analytical model for predicting the stiffness of threaded rods is proposed, accounting for different boundary conditions at the rod-ends.

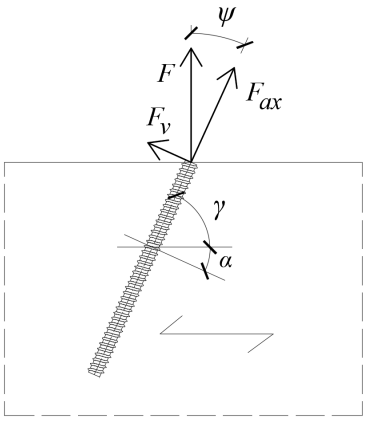

Fig. 2 Definition of terms used in the current investigation: F is the applied load, F_{ax} is the axial load component, F_v is the lateral load component, ψ is a load-to-rod angle, γ is a rod-to-grain angle, and α is a load-to-grain angle used for a calculation of embedment strength (f_h) according to Eurocode 5 (CEN 2004)

2. Materials and methods

2.1. Theoretical prediction of capacity and stiffness

2.1.1. Capacity

Axial capacity

The withdrawal capacity of long threaded rods is commonly specified by producers in their respective technical approvals. According to the producer of the rods used in the present investigation (SFS WB) (DiBt 2015), the withdrawal capacity can be determined by:

$$R_{ax,k} = 70 \cdot 10^{-6} \cdot \rho_k{}^2 \cdot d \cdot l_{ef} \tag{1}$$

where $R_{ax,k}$ is the characteristic withdrawal capacity, ρ_k is the characteristic value of the timber density, d is the outer diameter of threaded rods and l_{ef} is the effective length of rods screwed in timber. The relation is independent of the rod-to-grain angle γ, however, its validity is restricted to γ = 45-90°, and $4 \cdot d \le l_{ef} \le 1000\,\text{mm}$.

The current version of Eurocode 5 (CEN 2004) provides the following relation for the determination of withdrawal capacity of a single screw with d > 12 mm and $\gamma \ge 30°$:

$$R_{ax,k} = \frac{f_{ax,k} \cdot d \cdot l_{ef}}{1.2 \cdot \cos^2 \gamma + \sin^2 \gamma} \cdot \left(\frac{\rho_k}{\rho_a} \right)^{0.8} \tag{2}$$

where $f_{ax,k}$ is the characteristic withdrawal parameter perpendicular to the grain determined in accordance with EN14592 for the associated density ρ_a. Since $f_{ax,k}$ must be determined experimentally, the relation is of little practical use.

Stamatopoulos and Malo (2015) determined the withdrawal capacity of long threaded rods valid for γ = 0-90°. The proposed relation is based on the classical Volkersen theory (Volkersen 1938), which was applied for joints with bonded-in rods by (Gustafsson 1987; Johansson et al. 1995; Gustafsson 2000). The particular solution depends on the assumed mode of force transfer between the rod and the surrounding timber. For a general use of rods in joints, it is considered most appropriate to adopt the so-called pull-shear boundary conditions, yielding the following relations:

$$\frac{R_{ax,mean}}{\pi \cdot d \cdot l_{ef} \cdot f_w} = \left(\frac{\sin(m \cdot \omega \cdot \lambda_u)}{m \cdot \omega} + \frac{\tanh((1-\lambda_u) \cdot \omega) \cdot \cos(m \cdot \omega \cdot \lambda_u)}{\omega} \right) \tag{3}$$

$$\omega = \sqrt{\frac{\pi \cdot d \cdot \Gamma_e \cdot l_{ef}^2}{A_s \cdot E_s}};\ \Gamma_e = \frac{9.35}{1.5 \cdot \sin^{2.2}(\gamma) + \cos^{2.2}(\gamma)};$$
$$f_w = \frac{4.35}{0.91 \cdot \sin^2(\gamma) + \cos^2(\gamma)};\ m = \frac{0.332}{1.73 \cdot \sin(\gamma) + \cos(\gamma)} \tag{4}$$

where E_s is the elastic modulus of steel, A_s is the cross-sectional area of the threaded rod (with a thread root diameter) and the parameter λ_u is determined from a chart provided by Stamatopoulos and Malo (2015), or conservatively taken equal to 1.0. The material parameters are optimized for glulam class GL30c of Norway spruce.

Lateral capacity

Eurocode 5 (CEN 2004) adopts the European Yield Model (Johansen 1949), and it provides a set of relations for the determination of the lateral capacity (per fastener and shear plane) depending on the expected failure mode. The failure mode associated with the present investigation is a single plastic hinge in the fastener located in the timber member, giving the following relation:

$$R_{v,Rk} = \sqrt{2M_{y,Rk} \cdot f_{h,k} \cdot d_{ef}} + \frac{R_{ax,k}}{4} \tag{5}$$

where d_{ef} is the effective screw diameter, which for threaded rods is determined as $d_{ef} = 1.1 d_1$, $f_{h,k}$ is the characteristic embedment strength, and $M_{y,Rk} = 0.3 \cdot f_{u,k} \cdot d_{ef}^{2.6}$ is the characteristic fastener yield moment. For screws, the rope effect ($R_{ax,k} / 4$) is limited to 100 % of the Johansen's term. In the relation given in EC5, the Johansen's term is multiplied by a factor 1.15. This factor takes into account the different material safety factors (γ_M) for steel and timber, and it is not applicable when mean values are used.

For axially and laterally loaded self-tapping screws, Jockwer et al. (2014) proposed a modification of the Johansen's relation, assuming that timber does not resist lateral loads of screws within a distance x_1 from the timber edge:

$$R_{v,pulling} = -f_h \cdot x_1 \cdot d_{ef} + \sqrt{\left(2M_y + f_h \cdot x_1^2 \cdot d_{ef}\right) f_h \cdot d_{ef}} \tag{6}$$

$$x_1 = \frac{f_h \cdot d_{ef}}{2 \tan(\gamma) \cdot f_{v,roll}} \tag{7}$$

where $f_{v,roll}$ is the rolling shear strength. A mean embedment strength proposed by Blaß et al. (2006) was used by Jockwer et al. (2014):

$$f_{h,mean} = \frac{0.022 \cdot \rho^{1.24} \cdot d^{-0.3}}{2.5 \cdot \cos^2(\gamma) + \sin^2(\gamma)} \tag{8}$$

While the relation in Eq. (8) was obtained by curve-fitting to the experimental results with self-tapping screws of d = 6-12 mm, Eurocode 5 (CEN 2004) suggests to determine the value of the embedment strength f_h for screws with d > 6mm as:

$$f_{h,\alpha,k} = \frac{0.082(1-0.01\cdot d_{ef})\rho_k}{k_{90}\cdot \sin^2(\alpha)+\cos^2(\alpha)} \tag{9}$$

where k_{90} is, for softwoods, determined as $k_{90} = 1.35 + 0.015 \cdot d_{ef}$, and α is defined in Eurocode 5 as the angle of the load to the grain (the characterisation of α for the current investigation is depicted in Fig. 2).

Capacity under combined axial and lateral loading

According to Eurocode 5 (CEN 2004), axially and laterally loaded screws shall satisfy the following condition:

$$\left(\frac{F_{ax}}{R_{ax}}\right)^2 + \left(\frac{F_v}{R_v}\right)^2 \leq 1 \tag{10}$$

where F_{ax} and F_v are the load components in axial and lateral directions, respectively. By defining ψ as the angle between the rod axis and the resultant force (see Fig. 3a), the resultant force can be decomposed such as $F_{ax} = F \cdot \cos(\psi)$ and $F_v = F \cdot \sin(\psi)$, which inserted into Eq. (10), gives the following relation for the capacity R under combined axial and lateral loading:

$$R = \frac{R_{ax}\cdot R_v}{\sqrt{{R_{ax}}^2 \cdot \sin^2(\psi) + {R_v}^2 \cdot \cos^2(\psi)}} \tag{11}$$

Based on work of Bejtka and Blaß (2002), Jockwer et al. (2014) proposed to determine the capacity under combined axial and lateral loading for inclined screws as:

$$R = R_{ax,ef} \cdot \cos(\psi) + R_{v,pulling} \cdot \sin(\psi) \tag{12}$$

where $R_{ax,ef}$ is the withdrawal capacity determined with reduced effective length of screw by subtracting the length x_1 (Eq.(7)) from l_{ef}.

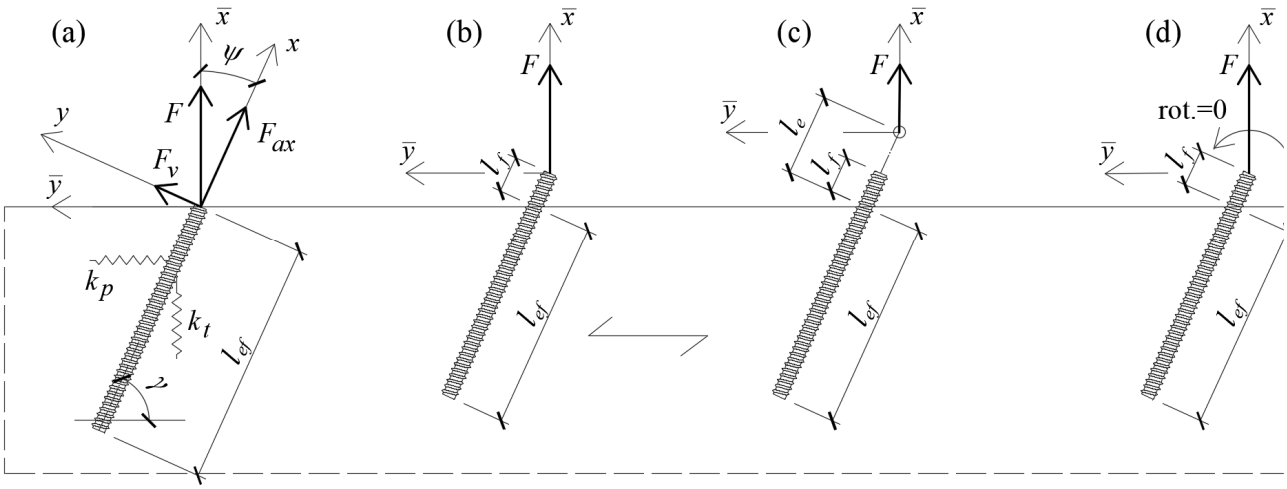

Fig. 3 Definition of terms in conjunction with stiffness prediction: (a) loading of the rod-end at the level of timber face, (b) loading of the rod-end eccentric to the timber face, (c) eccentric loading corresponding to the experimental set-up (see Section 2.2), (d) eccentric loading with restrained rotation (rot. = 0) of the rod-end

2.1.2. Stiffness

Axial stiffness

The axial withdrawal stiffness of threaded rods can be determined based on the classical Volkersen theory (Volkersen 1938), which was used by (Gustafsson 1987; Johansson et al. 1995; Gustafsson 2000) for bonded-in rods and by Jensen et al. (2001) for glued-in hardwood dowels and later applied for threaded rods by Stamatopoulos and Malo (2016):

$$K_w = \pi \cdot d \cdot l_{ef} \cdot \Gamma_e \cdot \frac{\tanh(\omega)}{\omega} \tag{13}$$

The input parameters, by assuming a pull-shear boundary conditions, are defined in Eq. (4).

Neither the technical approval (DiBt 2015), nor Eurocode 5 (CEN 2004) provides a relation for determining the axial withdrawal stiffness of long threaded rods. Some expressions can be found in other technical approvals for self-tapping screws. However, these expressions cannot be extrapolated outside their valid range as they provide inaccurate predictions (Stamatopoulos 2016).

The axial stiffness of the free part of the rod not embedded in timber is determined as $K_{ax,f} = E_s \cdot A_s / l_f$, where l_f is the free part of the rod, see Fig. 3. The total axial stiffness in the rod direction K_{ax} is obtained by:

$$K_{ax} = \frac{K_w \cdot K_{ax,f}}{K_w + K_{ax,f}} \tag{14}$$

Lateral stiffness

To the authors' knowledge, there are no studies dealing with the lateral stiffness of long threaded rods. Eurocode 5 (CEN 2004) provides only a general relation for determining the total slip of a steel-to-timber joint with dowels, bolts, screws or nails, as $K_{ser} = 2 \cdot \rho_m^{1.5} \cdot d / 23$ (per shear plane and fastener).

It is here proposed to estimate the lateral stiffness of long threaded rods by considering the rod as a semi-infinite beam supported on an elastic foundation, similar to studies dealing with the application of self-tapping screws as shear connectors in timber-to-concrete joints (Symons et al. 2010; Moshiri et al. 2014). The main advantage of the proposed method is a straightforward analytical determination of the lateral stiffness for different boundary conditions imposed at the end of the rod.

The differential equation for the deflection curve of a beam supported on elastic foundation is:

$$EI \frac{d^4 v}{dx^4} = -k \cdot v \tag{15}$$

where k is the foundation stiffness (N/mm^2) and EI represents the flexural stiffness of the beam. By introducing a parameter $\lambda = \sqrt[4]{k / (4EI)}$ and solving the differential equation with boundary conditions corresponding to the arrangement shown in Fig. 4 (the rod-end is loaded by a force P_0 and a moment M_0), the lateral displacement v_0 and rotation θ_0 at the rod-end become (Hetényi 1946):

$$v_0 = \frac{2P_0 \cdot \lambda}{k} + \frac{2M_0 \cdot \lambda^2}{k}$$
$$\theta_0 = \frac{2P_0 \cdot \lambda^2}{k} + \frac{4M_0 \cdot \lambda^3}{k} \tag{16}$$

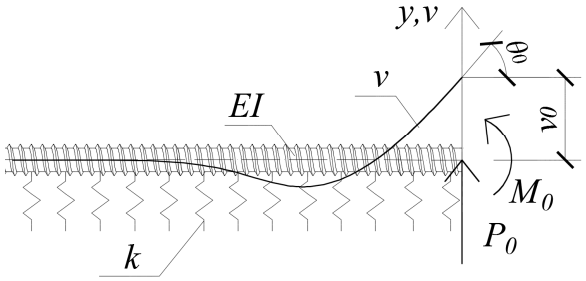

Fig. 4 Laterally loaded threaded rod considered as a semi-infinite beam on an elastic foundation

The lateral stiffness of the threaded rod K_v, in accordance with the configuration shown in Fig. 3a, can readily be obtained by inserting Eq. (16) with $M_0 = 0$ into a common force-displacement relation, and defining the flexural stiffness of rods as $EI = E_s \cdot \pi \cdot d_1^4 / 64$, giving:

$$K_v = \frac{k}{2\lambda} = \frac{d_1}{4}\sqrt[4]{\pi \cdot E_s \cdot k^3} \tag{17}$$

where d_1 is the root diameter of the threaded rods, E_s is the elastic modulus of steel and k is the foundation modulus of timber. The modulus k is obtained in correspondence with Eq.(21) by a simple interaction of foundation moduli of timber longitudinal to the grain, k_l, and transverse to the grain, k_t, as:

$$k = \frac{k_l \cdot k_t}{k_l \cdot \cos^2(\gamma) + k_t \cdot \sin^2(\gamma)} \tag{18}$$

Note that in this simplification, the rod is approximated as semi-infinite.

Modification of the lateral stiffness for various boundary conditions

The application of long threaded rods in moment resisting connections implies different boundary conditions at the rod-ends, as shown in Fig. 3. If the rods are fastened to steel connectors at a distance from the timber face (see Fig. 1), the total displacement at the end of the rods is the result of the deformations of the rod part embedded in timber and the free part of the rod. The lateral stiffnesses at the rod-end associated with the boundary conditions shown in Fig. 3 are given in the following, and the derivation of the relations can be found in Appendix A (Online resource).

The lateral stiffness corresponding to the configuration illustrated in Fig. 3c (representing the boundary conditions in the experimental set-up, see Section 2.2) is found by:

$$K_v = \frac{3kEI}{6EI\left(2l_e^2\lambda^3 + 2l_e\lambda^2 + \lambda\right) + kl_f\left(l_f^2 - 3l_f l_e + 3l_e^2\right)} \tag{19}$$

The lateral stiffness corresponding to the case illustrated in Fig. 3b can simply be obtained by Eq. (19) for $l_e = l_f$.

If the rotation at the end of the rod is restrained (Fig. 3d), the lateral stiffness is obtained by:

$$K_v = \frac{12kEI\left(4EI\lambda^3 + kl_f\right)}{48\left(EI\right)^2\lambda^4 + 8kEI\lambda l_f\left(2l_f^2\lambda^2 + 3l_f\lambda + 3\right) + k^2 l_f^4} \tag{20}$$

Resultant stiffness in the load direction

The respective stiffnesses in the axial K_{ax} and lateral direction K_v are associated with the coordinate system of the rod $x-y$, see Fig. 3a. The resultant stiffness in the load direction is found by a transformation of the rod coordinate system into a coordinate system associated with loading, $\bar{x}-\bar{y}$, by applying a rotation ψ. The force-displacement relation in the rod coordinate system $x-y$, $\mathbf{F}=\mathbf{K}\cdot\boldsymbol{\delta}$, is transformed to the coordinate system $\bar{x}-\bar{y}$ by use of rotation tensor **Q,** such that $\overline{\mathbf{K}}=\mathbf{Q}\cdot\mathbf{K}\cdot\mathbf{Q}^T$, $\overline{\mathbf{F}}=\mathbf{Q}\cdot\mathbf{F}$ and $\overline{\boldsymbol{\delta}}=\mathbf{Q}\cdot\boldsymbol{\delta}$. The set of equations $\overline{\mathbf{F}}=\overline{\mathbf{K}}\cdot\overline{\boldsymbol{\delta}}$ is solved for the displacement along $\bar{x}$, $\bar{\delta}_x$, and the stiffness in the load direction is found by $K=F/\bar{\delta}_x$ as:

$$K = \frac{K_{ax}\cdot K_v}{K_{ax}\cdot\sin^2(\psi) + K_v\cdot\cos^2(\psi)} \tag{21}$$

If displacements along $\bar{y}$ are prevented ($\bar{\delta}_y = 0$), the stiffness in the load direction reads:

$$K = K_{ax}\cdot\cos^2(\psi) + K_v\cdot\sin^2(\psi) \tag{22}$$

It can be noted that the relation given in Eq. (21) is a variation of Hankinson's formula, and furthermore that Eq. (22) corresponds to the relation proposed by Tomasi et al. (2010) for stiffness prediction of timber-to-timber lap connections with inclined self-tapping screws.

2.2. Experimental tests

The effects of rod-to-grain angle combined with different load and rod axis directions on capacity and stiffness were investigated experimentally. The experimental tests were carried-out with a pull-beam test configuration. The experimental set-up is shown in Fig. 5. A purpose-made steel coupler was screwed onto the tip of the rods and connected to the load actuator through a bolt, hence forming a hinge allowing free rotation. The bolt location was used as a reference point for the displacement monitoring. The displacement was measured by 4 displacement transducers (LVDT). One pair of LVDTs was oriented vertically (TV), whereas the other pair was oriented horizontally (TH) (in the initial configuration, i.e. before loading). In each pair, the LVDTs were placed at the opposed sides of the timber beam. The mean value of the measurements was used in the evaluation. The vertical LVDTs were attached to the lower face of the beam, whereas the horizontal LVDTs were attached to a fixed point distant to the timber beams. Free rotation at the ends of the LVDTs was provided. The relative displacement in the vertical direction (perpendicular to the grain with reference to the timber beam), which is of interest in the current investigation, can be calculated knowing the distances between the reference points of LVDTs in the initial configuration. In addition, the horizontal displacement of the beam was monitored and was found to be insignificant.

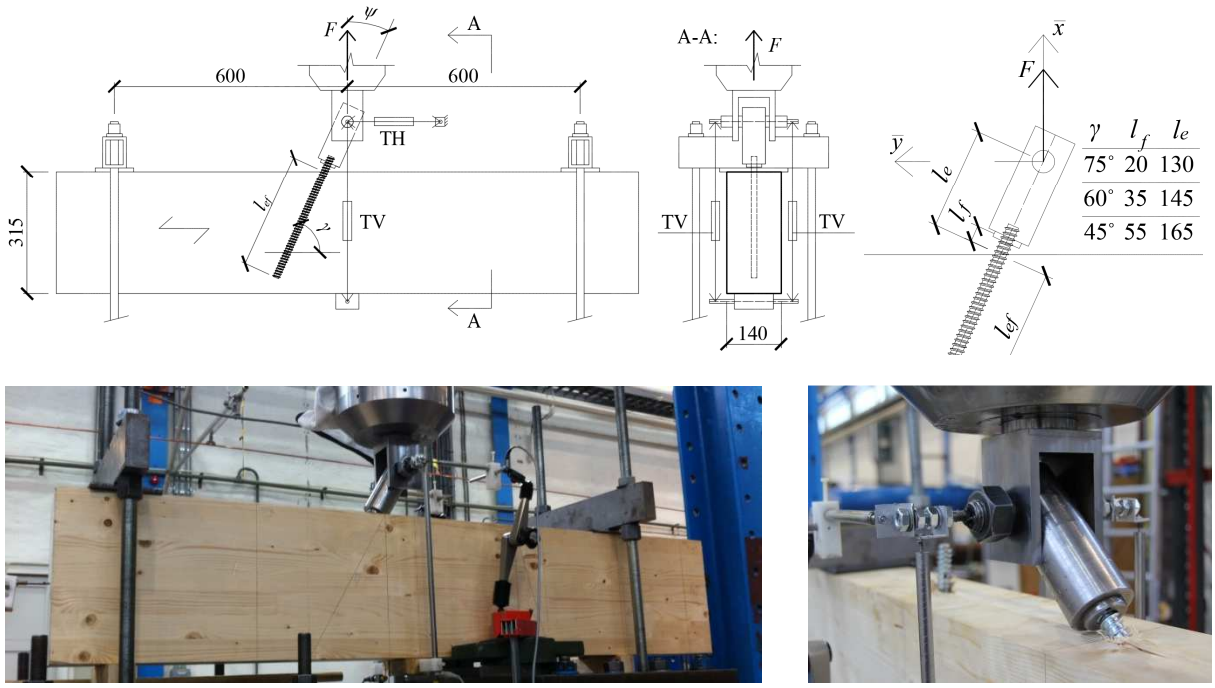

Fig. 5 Experimental set-up

The load was applied in perpendicular to the grain direction with a constant displacement rate of 2 mm/min. The load actuator was fixed through a hinge to a steel frame at a vertical distance of approximately 2.5 m from the timber beam. Since the horizontal displacement of the rod is of the order of millimeters, the applied force can be assumed acting vertically (the horizontal force component is negligible). Five tests were carried-out for specimens with rod-to-grain angles γ = 60˚ and 75˚, and one additional test was performed for γ = 45˚, leading to load-to-rod angles ψ=90˚-γ.

The timber beams were made of glulam strength class GL30c (CEN 2013) and had 140 mm width and 315 mm height. The beams were fabricated with 45 mm thick lamellas of Norway spruce (Picea Abies). The timber specimens were conditioned at the standard environment of 20º C and 65 % relative humidity, resulting in approximately 12 % moisture content.

The threaded rods were of type SFS WB-T-20 (DiBt 2015) complying with DIN 7998 (DIN 1975). The outer diameter of the rods, d, was 20 mm, whereas the inner diameter, d_1, was 15 mm. The strength class was 8.8 according to the manufacturer. The effective (embedment) length of the rods l_{ef} was 300 mm in all tests.

2.3. Numerical model

Numerical simulations were carried out by ABAQUS (DSS 2014). Three models corresponding to the experimental configurations (γ = 45˚, 60˚ and 75˚) were used in order to determine the stiffness in direction of the applied load, see Fig. 6. The coupling steel part between the rod and the load actuator, used in the experiments, has much higher flexural and axial stiffness compared to the rods, and it was therefore omitted in the numerical models. The load was applied in perpendicular to the grain direction through a distant reference point coupled rigidly to the rod-end. In addition, three models with no eccentricity of the load, and the rod-end located at the level of the upper timber face (case (a) in Fig. 3), were used for verification of the proposed analytical model. Out-of-the-plane displacements were prevented at the reference point used for the load application. The timber beams were supported by removing all translational degrees of freedom at the support regions (at locations in correspondence with the experiments).

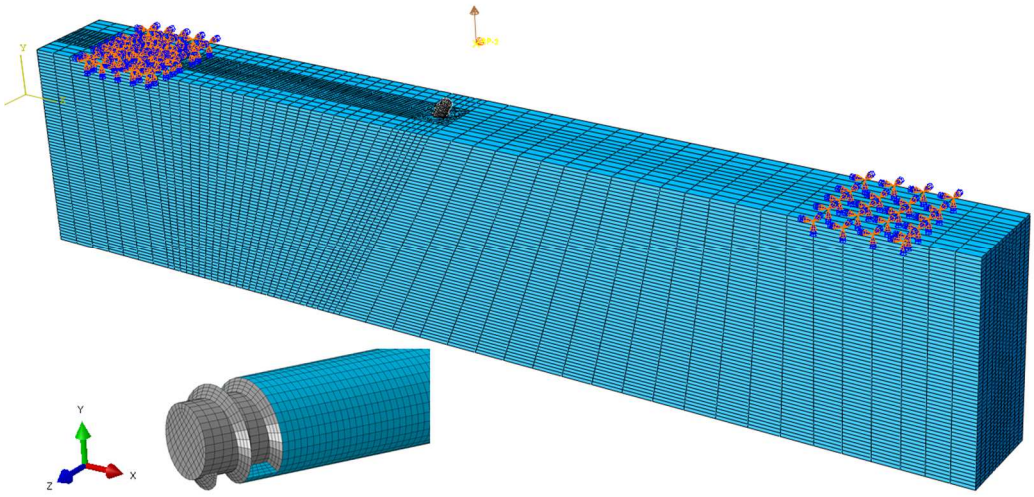

Fig. 6 Numerical model

Eight-node brick elements with reduced integration and hour-glass control (C3D8R) were used in the models. A sensitivity study was carried out in order to determine a satisfactory mesh size. The mesh was denser in the vicinity of the rods. The rod and its interaction with the timber was based on a numerical model presented by Stamatopoulos and Malo (2016). Contact properties between rod and timber utilized a "hard" contact behaviour in the normal direction and isotropic tangential behaviour with a coefficient of friction of 0.2, which was based on the study by Koubek and Dedicova (2014).

The numerical models were used solely to simulate the behaviour in the elastic domain (the stiffness prediction was of interest here). Therefore, only elastic material properties were applied without any failure criterion or damage law. Wood was modelled as transversally isotropic with the material properties summarized in Table 1. Here, E is the modulus of elasticity, G is the shear modulus and v is the Poisson's ratio. The longitudinal direction (L) is the grain direction, and no distinction is made between tangential (T) and radial (R) directions. Steel was modelled as isotropic with E = 210 GPa and v = 0.3.

Table 1 Material properties of wood used in numerical simulations

E_L [MPa] [(a)]	E_R=E_T [MPa] [(a)]	G_{LR}=G_{LT} [MPa] [(b)]	G_{RT} [MPa] [(b)]	v_{LR}=v_{LT} [-] [(b)]	v_{TR} [-] [(b)]
13000	400	600	30	0.6	0.315

[(a)] Manufacturer: Moelven industrier ASA, class L40 (GL30c)

[(b)] Norway spruce – estimations based on (Dahl 2009)

3. Results and discussion

3.1. Experimental results

The average values of the ultimate force F_u and the stiffness in the load direction K are presented in Table 2.

Table 2 Experimental results in terms of the ultimate force F_u and the stiffness K (COV: coefficient of variation)

γ	No.of tests	F_u		K	
		[kN]	COV	[N/mm]	COV
75˚	5	85	0.10	7300	0.09
60˚	5	64	0.16	1200	0.13
45˚	1	49	-	390	-

Note: $\gamma+\psi = 90^\circ$

The stiffness was obtained by linearization of the initial elastic part of the force-displacement curves shown in Fig. 7, which is limited to approximately 4, 8 and 10 mm, respectively for the rod-to-grain angles of γ = 75, 60 and 45˚. For larger load-to-rod angles (confer results for specimens with γ = 60 and 45˚), it is observed that after the initial elastic part, yielding in the steel rods propagates due to bending, characterized by a decreasing stiffness. Finally, the rod-ends are eventually bended (rotated) towards the direction of the applied force. This phase is characterized by a steep increase in stiffness and "opening" of the timber specimens in close proximity to the point where the rods penetrate the timber beams, see Fig. 7. The failure is finally reached due to withdrawal of the rods.

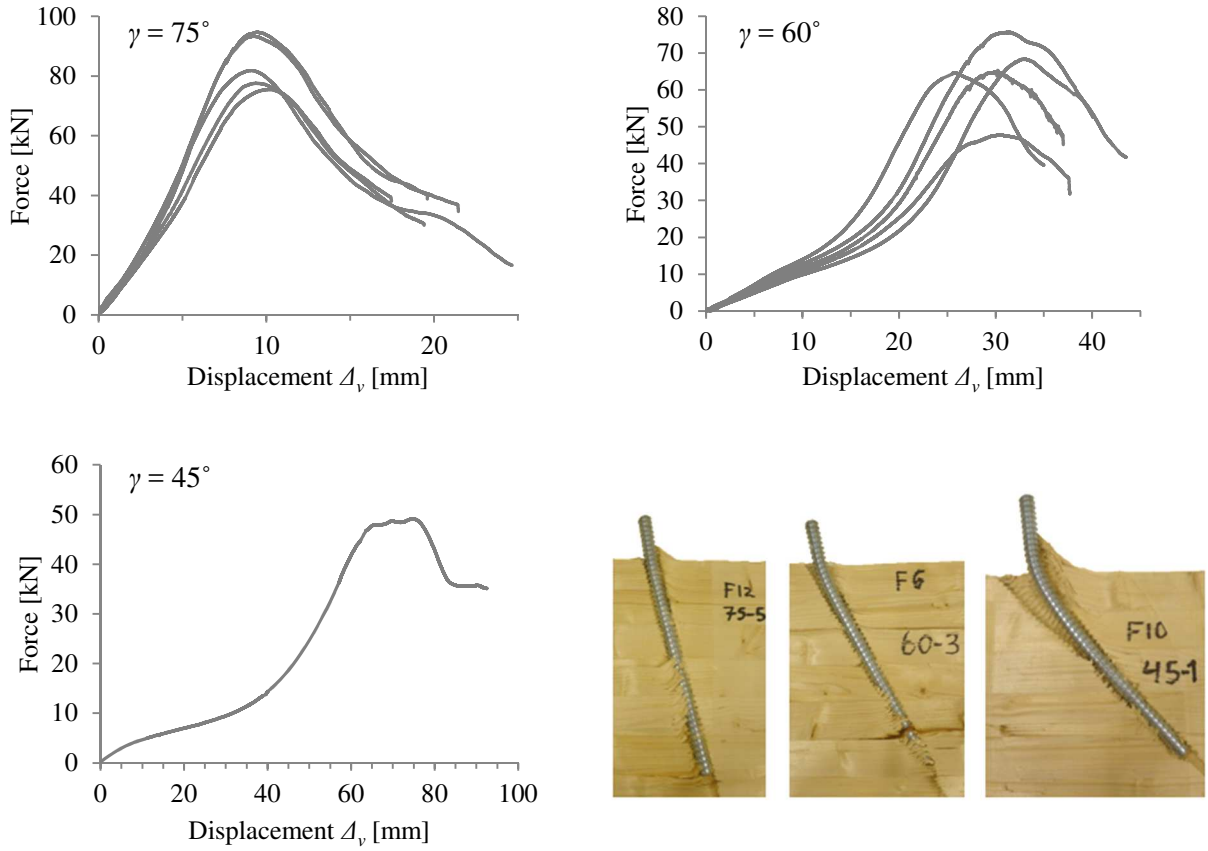

Fig. 7 Experimentally obtained force-displacement curves and examples of cut-opened specimens after testing; Δv is a vertical displacement (in the direction of the applied force). Note: $\gamma+\psi = 90^\circ$

3.2. Theoretically predicted capacity and stiffness compared to experimental results

3.2.1. Capacity

The ultimate force obtained from the experiments is compared with the analytically predicted values. Two different analytical models were used, see Table 3. Model 1 represents the capacity prediction by Eurocode 5 (CEN 2004). Model 2 utilizes the design model for self-tapping screws presented by Jockwer et al. (2014) with two different embedment strengths f_h. In both models, the axial capacity by the producers' technical approval (TA (DiBt 2015)) was used. As shown in Table 4, the axial capacity obtained by use of Eq. (3) (Stamatopoulos and Malo 2015) is very similar to the values obtained by the prediction of TA, resulting in minor variations of the total capacity. It should, however, be kept in mind that the use of TA is not valid for rod-to-grain angles $\gamma < 45°$.

Table 3 Definition of the analytical models used for the capacity prediction

Model	R_{ax}	R_v	f_h	R
M.1	SFS TA Eq.(1)	EC5 Eq.(5)	EC5 Eq.(9)	EC5 Eq.(11)
M.2a	SFS TA [(a)] Eq.(1)	Jockwer et al. Eq.(6)	Blaß et al. Eq.(8)	Jockwer et al. Eq.(12)
M.2b	SFS TA [(a)] Eq.(1)	Jockwer et al. Eq.(6)	EC5 Eq.(9)	Jockwer et al. Eq.(12)

[(a)] with l_{ef} reduced by x_1

The results obtained by the analytical models and the experiments are summarized in Table 4. Mean values of the input parameters were used in the calculations in order to obtain the capacity mean values. The mean value of $f_{v,roll,m}$ was obtained by modifying the characteristic strength for glulam of $f_{v,roll,k}$ = 1.2 MPa (CEN 2013) by COV = 0.15, which was taken from (JCSS 2006). The mean value of $f_{u,m}$ was obtained from test results by Stamatopoulos and Malo (2015), for which the mean tensile capacity of the threaded rods was found to be 176 kN (d_{ef} was used in the calculations). The mean density of timber ρ_m is declared by the producer of the glulam specimens. The value corresponds well to experiments carried out earlier with the same glulam class (Cepelka and Malo 2016).

Table 4 Comparison of mean capacity obtained by the analytical models and the experiments

γ	$R_{ax,m}$ [kN]		$R_{v,m}$ [kN]			R_m, F_u [kN]			
	Eq.(3)	Eq.(1)	M.1	M.2a	M.2b	M.1	M.2a	M.2b	Exp.(F_u)
90°	89.6	92.8	41.1	15.5	20.5	92.8	92.8	92.8	97 [(a)]
75°	89.1	92.8	40.3	9.6	7.7	81.7	85.0	78.4	85
60°	87.5	92.8	38.3	7.0	4.4	62.3	72.8	59.5	64
45°	85.3	92.8	36.1	5.5	2.9	47.5	57.3	38.8	49

[(a)] Mean experimental capacity taken from (Stamatopoulos and Malo 2015)
Input to the anal. models: ρ_m = 470 kg/m^3, E_s = 210 GPa, $f_{v,roll,m}$ = 1.55 MPa, $f_{u,m}$ = 905 MPa, l_{ef} = 300 mm, d_1 = 15 mm, d = 20 mm
Note: $\gamma+\psi = 90°$

The graphical visualization of the results in Fig. 8 (left) shows clearly that both design models yield good estimates of the ultimate force. For the design model of Jockwer et al. (2014), it seems to be more appropriate to use embedment strengths f_h based on Eurocode 5. The effect of the rod inclination on the capacity as obtained by the experiments is shown in Fig. 8

(right). The rod-to-grain angle $\gamma = 45^\circ$ leading to load-to-rod angle $\psi = 45^\circ$ results in approximately 50 % reduction of the capacity compared to the capacity under pure axial loading normal grain $F_{u,90}$.

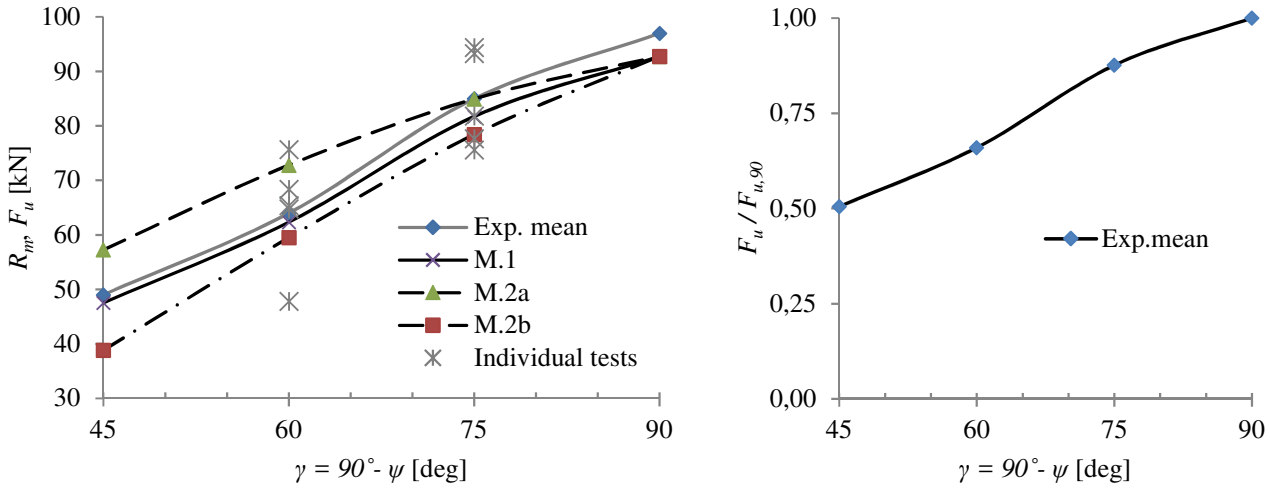

Fig. 8 Left: Comparison of capacity obtained by the analytical models and the experiments, Right: Effect of the rod-to-grain angle γ and load-to-rod angle $\psi = 90^\circ - \gamma$ on the capacity

3.2.2. Stiffness

Summary of mean experimental, analytical and numerical results of the stiffness in the load direction is presented in Table 5. Two different boundary conditions are analysed herein. The first set of results, $K^{(c)}$, is associated with the configuration used in the experiments (Fig. 3c). The second set, $K^{(a)}$, is associated with a basic configuration, for which the load is acting with no eccentricity from the timber member (Fig. 3a). The analytical prediction of $K^{(c)}$ was obtained by use of set of Eqs. (14), (19) and (21), while for the prediction of $K^{(a)}$, Eqs. (13), (17) and (21) were used. The values of $K^{(a)}$ obtained by the proposed analytical and numerical models are furthermore compared to the model by Jockwer et al. (2014). For joints with inclined self-tapping screws, Jockwer et al. (2014) proposed to determine the stiffness in the load direction (for load acting perpendicular to the grain) as an effective stiffness of springs in series: $K_{90} = K_{ax} \cdot K_{v,pulling} / (K_{ax} + K_{v,pulling})$, where $K_{v,pulling} = 3 \cdot E_s \cdot \pi \cdot d_1^4 / (64 \cdot x_1^3)$ represents the lateral stiffness (x_1 is obtained by Eq. (7)), while K_{ax} represents the axial withdrawal stiffness of the screw.

Table 5 Comparison of mean stiffness obtained by experiments, analytical and numerical models

γ	$K^{(c)}$ - test config. [N/mm]			$K^{(a)}$ - no eccentricity [N/mm]		
	Exp.	Anal.	Num.	Anal.	Num.	Anal. [(1)]
75°	7300	6600	7300	76800	72700	51500
60°	1200	1300	1200	50150	46000	18300
45°	390	430	440	30600	26600	8200

[(1)] Model by Jockwer et al. (2014)

Input to the anal. models: $\rho_m = 470$ kg/m^3, $E_s = 210$ GPa, $f_{v,roll,m} = 1.55$ MPa, $d = 20$ mm, $d_1 = 15$ mm, $l_{ef} = 300$ mm, $k_t = 710$ MPa, $k_l = 1300$ MPa, l_f and l_e see Fig. 5

Note: $\gamma + \psi = 90^\circ$

The mean values of input parameters were used in order to obtain the mean stiffness. The foundation moduli transverse (k_t) and longitudinal (k_l) to the grain were taken as the average of experimental results for spruce and steel dowels (diameter 16 mm) from investigations by Gattesco (1998) and Gattesco and Toffolo (2004). The remaining input parameters are discussed in Section 3.2.1.

The values of the stiffness $K^{(c)}$ obtained by the proposed analytical model show good agreement with the experimental results, confer Table 5. The numerical models predict very well the stiffness $K^{(c)}$ compared to the experimental results, and can thus be used as a validation for the analytically obtained $K^{(a)}$. Good agreement between numerical simulations and the results obtained from the proposed model is here achieved, while the model proposed by Jockwer et al. (2014) gives too low stiffness as shown graphically in Fig. 9 (left). Embedment strength f_h according to Blaß et al. (2006) was used in the analytical prediction by Jockwer et al. (2014). The use of f_h according to Eurocode 5 yields even lower values of the predicted stiffness. Besides the underestimation of the stiffness prediction for the basic case (case (a)), the model by Jockwer et al. (2014) cannot be directly used for other boundary conditions at the rod-ends and it is therefore not suitable for the use for long threaded rods in joints.

The effect of the rod inclination relative to the grain and loading direction on the stiffness $K^{(a)}$ obtained by the proposed analytical model is shown in Fig. 9 (right). The rod-to-grain angle $\gamma = 45^\circ$ leading to load-to-rod angle $\psi = 45^\circ$ results in approximately 70 % reduction of the stiffness compared to pure withdrawal stiffness normal grain $K_{w,90}$.

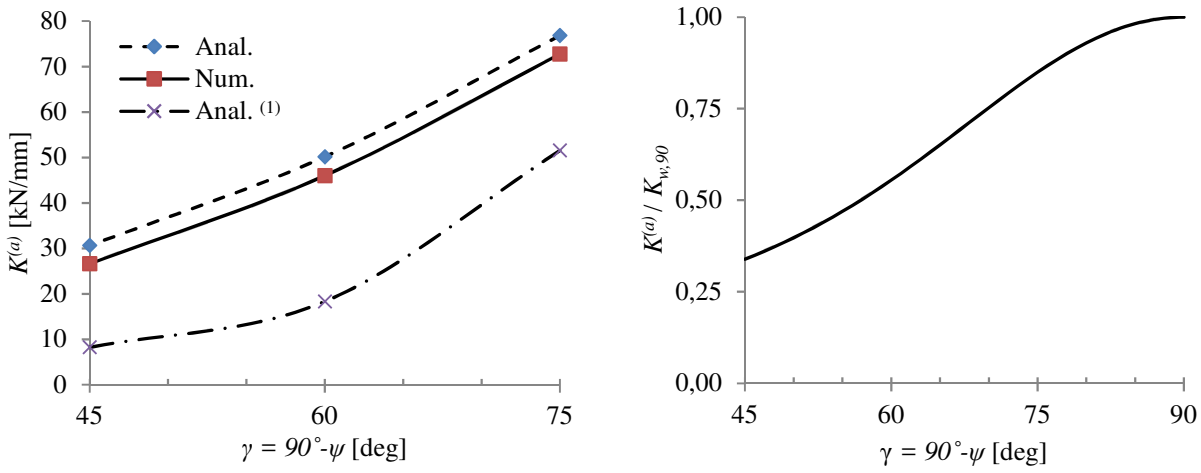

Fig. 9 Left: Comparison of stiffness $K^{(a)}$ obtained by numerical and analytical models, Right: Relation $K^{(a)}/K_{w,90}$ obtained by the proposed analytical model; (1) Model by Jockwer et al. (2014)

The influence of the boundary conditions and the extent of the free length of rod not embedded in timber l_f are studied in Fig. 10. The stiffness corresponding to the boundary conditions illustrated in Fig. 3b, $K^{(b)}$, was calculated with varying free lengths of rod l_f = 0, 10, 20, 30 and 40 mm. The comparison of $K^{(b)}$ with pure axial withdrawal stiffness normal grain is shown in Fig. 10 (left) as ratios $K^{(b)}/K_{w,90}$. Similarly, Fig. 10 (middle) shows the ratios of $K^{(d)}/K_{w,90}$, where $K^{(d)}$ is the stiffness corresponding to the boundary conditions illustrated in Fig. 3d. The comparison of Fig. 10 (left) and (middle) illustrates the significant effect of the rotational restraint at the end of the rod (case (d)). A considerably better performance, in terms of stiffness, can be achieved by restraining the displacement at the end of the rod, transversally to the loading (stiffness obtained by Eq. (22)), as demonstrated in Fig. 10 (right). It can moreover be noticed that, in such a configuration, the effect of the rotational restraint nearly vanishes.

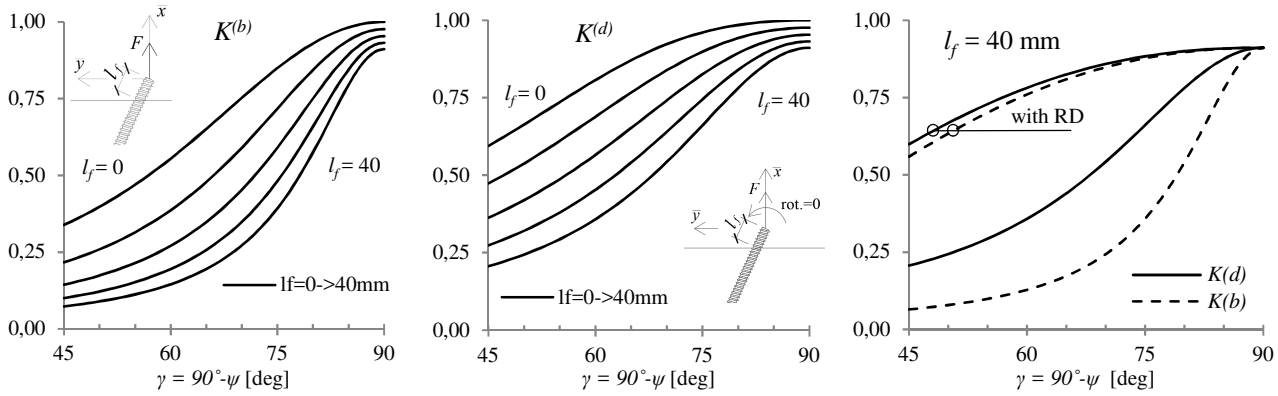

Fig. 10 Influence of boundary conditions and length l_f on the stiffness: Left: $K^{(b)}/K_{w,90}$, Middle: $K^{(d)}/K_{w,90}$, Right: effect of the restrained displacement (RD) at the rod-end transversally to the loading

4. Concluding remarks

The effect of rod-to-grain and load-to-rod angles on capacity and stiffness of axially and laterally loaded long threaded rods used as connectors in timber joints was investigated by use of experiments and numerical models. Analytical relations are proposed for determining the capacity and the stiffness. The main findings are summarized in the following:

- Both capacity and stiffness of the threaded rods are significantly reduced by the increased rod-to-grain and load-to-rod angles. The rod-to-grain angle of 45˚, leading to load-to-rod angle of 45˚ in the current investigation, resulted in approximately 50 % reduction of the capacity and 70 % reduction of the stiffness compared to pure axial loading normal grain.
- Analytical prediction of capacity can be carried out by use of relations in Eurocode 5 (CEN 2004) or the model proposed by Jockwer et al. (2014) for connections with inclined screws. Both models yield good estimation of the ultimate load for varying rod-to-grain angle compared to the experimental results.
- An analytical model for predicting the stiffness is proposed and validated by experimental results and finite element simulations. The model can readily be modified for different boundary conditions at the rod-ends. Analytical relations are derived, associated with four different boundary conditions applicable for joints.
- In timber joints with threaded rods fastened to steel couplers, an increased stiffness of the rods can be obtained by restraining the rotation at the rod-ends. Significant increase of stiffness is achieved providing support at the rod-end transversally to the load direction (e.g. by anchoring the steel couplers to the timber member).

Acknowledgment

This work was funded by the WoodWisdom-Net+ project DuraTB (“Durable Timber Bridges”) and the support from the funding bodies and partners is gratefully acknowledged. The authors would also like to acknowledge Halvor Grytting and Eirik Dimmen Sæle for their important contributions and good experimental work.

References

Bejtka I, Blaß HJ Joints with inclined screws. In: CIB W18-Meeting 35, Kyoto, Japan, 2002. pp Paper 7-5

Blaß HJ, Bejtka I, Uibel T (2006) Tragfähigkeit von Verbindungen mit selbst bohrenden Holzschrauben mit Vollgewinde (Load capacity of connections with self-drilling wood screws with full thread). Universität Karlsruhe, Karlsruhe: KIT Scientific Publishing

Blaß HJ, Krüger O (2010) Schubverstärkung von Holz mit Holzschrauben und Gewindestangen (Shear reinforcement of wood with wood screws and threaded rods). Universität Karlsruhe, Karlsruhe: KIT Scientific Publishing

CEN (2004) EN 1995-1-1:2004: Design of timber structures. Part 1-1: General-Common rules and rules for buildings. European committee for standarization, Brussels

CEN (2013) EN 14080:2013: Timber structures-Glued laminated timber and glued solid timber - Requirements. European Committee for Standardization,

Cepelka M, Malo KA Experimental study of end grain effects in timber joints under uniaxial compression load. In: J. Eberhardsteiner WW, A. Fadai, M. Pöll (ed) Proceedings of World Conference on Timber Engineering (WCTE 2016), August 22-25, 2016, Vienna, Austria, 2016. Vienna University of Technology, Austria, ISBN: 978-3-903039-00-1

Dahl KB (2009) Mechanical properties of clear wood from Norway spruce. Dissertation. Norwegian University of Science and Technology

DiBt (2015) Allgemeine bauaufsichtliche Zulassung - Z-9.1-777 - Gewindestangen mit Holzgewinde als Holzverbindungsmittel (General building approval - Z-9.1-777 - Threaded rods with wood threads as wood connectors). Deutches Institut für Bautechnik, Berlin

DIN (1975) DIN 7998: Gewinde und Schraubenenden für Holzschrauben (Threads and screws for wood). Deutsches Institut für Normung, Berlin

DSS DSSC (2014) Abaqus analysis user's guide, Version 6.14.

Gattesco N (1998) Strength and local deformability of wood beneath bolted connectors. Journal of Structural Engineering 124:195-202

Gattesco N, Toffolo I (2004) Experimental study on multiple-bolt steel-to-timber tension joints. Materials and Structures/Materiaux et Constructions 37:129-138

Gustafsson PJ (1987) Analysis of generalized Volkersen-joints in terms of non-linear fracture mechanics. In: Verchery G, Cardon H (eds) Mechanical behaviour of adhesive joints. Edition Pluralis, Paris, France, pp 323-338

Gustafsson PJ Predicting the pull-out strength of glued-in rods. In: Proceedings of the sixth World Conference on Timber Engineering, University of British Columbia, BC, Canada, 2000.

Hetényi M (1946) Beams on elastic foundation: Theory with applications in the fields of civil and mechanical engineering. The University of Michigan Press, Baltimore

JCSS (2006) JCSS Probabilistic model code, Part 3: Resistance models, 3.05: Timber

Jensen JL, Koizumi A, Sasaki T, Tamura Y, Iijima Y (2001) Axially loaded glued-in hardwood dowels. Wood Science and Technology 35:73-83 doi:10.1007/s002260000076

Jockwer R, Steiger R, Frangi A (2014) Fully Threaded Self-tapping Screws Subjected to Combined Axial and Lateral Loading with Different Load to Grain Angles. In: Aicher S, Reinhardt HW, Garrecht H (eds) Materials and Joints in Timber Structures: Recent Developments of Technology, RILEM Bookseries 9, vol 9. Springer Netherlands, Dordrecht, pp 265-272. doi:10.1007/978-94-007-7811-5_25

Johansen KW (1949) Theory of timber connectors. International Association of Bridges and Structural Engineering Publication No.9:249-262

Johansson C-J, Serrano E, Gustafsson PJ, Enquist B Axial strength of glued-in bolts. Calculation model based on non-linear fracture mechanics - a preliminary study. In: Proceedings of CIBW18, Meeting twenty-eight, Copenhagen, Denmark, 1995.

Koubek R, Dedicova K (2014) Friction of wood on steel. Master Thesis. Linnaeus University

Malo KA, Abrahamsen RB, Bjertnæs MA (2016) Some structural design issues of the 14-storey timber framed building "Treet" in Norway. European Journal of Wood and Wood Products 74:407-424 doi:10.1007/s00107-016-1022-5

Malo KA, Stamatopoulos H Connections with threaded rods in moment resisting frames. In: J. Eberhardsteiner WW, A. Fadai, M. Pöll (ed) Proceedings of the World Conference on Timber Engineering (WCTE 2016), August 22-25, 2016, Vienna, Austria, 2016. Vienna University of Technology, Austria, ISBN: 978-3-903039-00-1,

Moshiri F, Shrestha R, Crews K (2014) The Predictive Model for Stiffness of Inclined Screws as Shear Connection in Timber-Concrete Composite Floor. In: RILEM Bookseries, vol 9. pp 443-453. doi:10.1007/978-94-007-7811-5_40

Stamatopoulos H (2016) Withdrawal properties of threaded rods embedded in glued-laminated timber elements. Dissertation. NTNU, Norwegian University of Science and Technology

Stamatopoulos H, Malo KA (2015) Withdrawal capacity of threaded rods embedded in timber elements. Construction and Building Materials 94:387-397 doi:http://dx.doi.org/10.1016/j.conbuildmat.2015.07.067

Stamatopoulos H, Malo KA (2016) Withdrawal stiffness of threaded rods embedded in timber elements. Construction and Building Materials 116:263-272 doi:http://dx.doi.org/10.1016/j.conbuildmat.2016.04.144

Symons D, Persaud R, Stanislaus H (2010) Slip modulus of inclined screws in timber-concrete floors. Proceedings of the Institution of Civil Engineers: Structures and Buildings 163:245-255 doi:10.1680/stbu.2010.163.4.245

Tomasi R, Crosatti A, Piazza M (2010) Theoretical and experimental analysis of timber-to-timber joints connected with inclined screws. Construction and Building Materials 24:1560-1571 doi:http://dx.doi.org/10.1016/j.conbuildmat.2010.03.007

Volkersen O (1938) Die nietkraftverteilung in zugbeanspruchten nietverbindungen mit konstanten laschenquerschnitten (The rivet-force distribution in tension-stressed rivet joints with constant adherends thickness). Luftfahrtforschung 15